Assessing the topological structure of a smart low-voltage grid

Ebisa Negeri, Fernando Kuipers*, Nico Baken

Network Architectures and Services, Delft University of Technology, PO Box 5031, 2600 GA Delft, The Netherlands

Abstract

The electric power grid is a critical infrastructure that delivers electric power from electricity sources to consumers. Currently, renewable and distributed sources of electricity, as well as new technologies that introduce large loads, are significantly changing the load profiles at the low-voltage grid. This trend calls for reassessing the structure of the low-voltage grid to see if it can safely accommodate the new load profiles. Moreover, the future smart grid relies on ICT (Information and Communication Technology) networks to support decentralized power distribution. Yet, the nodes of the ICT networks might depend on the grid itself for power supply leading to bidirectional interdependence between the two networks, which might affect the reliability of the power grid.

The focus of this paper is to enhance the reliability of the future low-voltage grid, by improving the structure of the low-voltage grid itself as well as by identifying its interdependence with the ICT network. We investigate the structural features of the low-voltage grid and assess their influence on its capability to handle the new load profiles. We use concepts from complex networks theory to derive relevant structural metrics that characterize the structural properties of the low-voltage grid. We also propose performance metrics that reflect the operational performance of the low-voltage grid. We analyze different low-voltage networks under various loading scenarios to observe the influence of structural metrics of the low-voltage grid on its operational metrics. Based on this analysis, we propose a constraint programming formulation for cost-optimal and robust design of the struc-

*The corresponding author is Fernando Kuipers

Email addresses: e.o.negeri@tudelft.nl (Ebisa Negeri), F.A.Kuipers@tudelft.nl (Fernando Kuipers), N.H.G.Baken@tudelft.nl (Nico Baken)

ture of the low-voltage grid. In addition, based on our assessment of the interdependence level between the ICT and low-voltage networks, we propose a design algorithm for the dependency of ICT nodes on grid nodes to increase the reliability of the grid.

Keywords: Smart grid, topology, Complex network theory, ICT network, Interdependent networks.

---

1. Introduction

In the traditional electric power system, power is generated at large-scale generators. The generated power is stepped up to a high-voltage, typically 380 kV (kilo Volt) - 110 kV, and transported over long distance by the high-voltage transmission grid to the transmission sub-stations. At the transmission sub-stations, the power is stepped down to a medium-voltage which is typically in the range 10 kV - 20 kV. The power is then transported over the medium-voltage grid to the medium-voltage to low-voltage (MV/LV) transformers, where the power is further stepped down to low voltage (typically 230V) that is suitable for end consumers. The low-voltage grid distributes the power to the end customers.

In a classical low-voltage grid, the end consumers are connected to the transformer in a typical radial structure as shown in Fig. 1. This radial structure is designed for unidirectional supply of power from the transformer to the end consumers with small loads, such as residential loads.

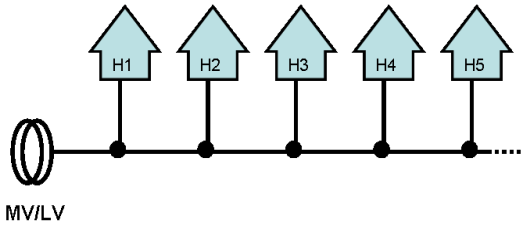

Figure 1: A typical radial low-voltage grid.

For safe operation of a low-voltage grid, the voltage levels at all the nodes and the loads in all the cables should be maintained within their respective operational boundaries. In a low-voltage grid, the voltage level at the transformer is stable, while the voltage levels at the other nodes can vary depending on the power flows. Under normal operation, the voltage

level at each node should remain within the range[1] of 90% - 110% of 230V. In addition, each cable in the low-voltage grid has a maximum load capacity that should not be exceeded. If these boundaries are violated, it can lead to deterioration of the quality of the power delivered, or even worse to network breakdown. Traditionally, the node voltages and cable loads are easily maintained within their operational ranges, because the low-voltage grid connects households with conventional appliances that present small loads to the grid.

However, the power grid is facing transitions. With the growing concerns for green energy, energy efficiency and energy security, distributed power sources, such as solar panels, wind turbines, micro-CHPs (combined heat and power plants), etc., are becoming widely available. As a result, end consumers of electricity are transforming to *prosumers* that can locally generate and feed their surplus power back to the grid. Moreover, new devices such as electric vehicles and heat-pumps that introduce large load are becoming increasingly available. As more distributed resources become available, it is foreseeable that decentralized energy exchanges take place on the power grid. These decentralized power exchanges involve information flow among different elements in the grid. Accordingly, it is likely that communication networks will be deployed at all levels of the power grid to support the information flows in the system [1]. When low-voltage grid depends on ICT networks, the nodes of the ICT network could at the same time depend on the grid itself for their power supply.

These new developments in the power system will revolutionize the low-voltage grid, because it is the part of the power grid where most of the distributed energy sources and new devices will be connected. Although the low-voltage grid is traditionally a passive part of the power grid where passive small-scale end consumers are connected, its role and relevance will increase with these new developments.

These transitions also raise different concerns. One of the concerns is that the structure of the low-voltage grid that was originally designed for supplying power to the traditional passive consumers might not be able to support the new load profiles. The challenge is whether the low-voltage grid can maintain safe operational boundaries of the node voltages and the cable loads. Although the classical residential loads usually do not cause significant voltage drops and stresses on the cables, the power injected back to the grid from the prosumers as well as the large loads of electric vehicles

[1]This is the standard in most European countries.

and heat-pumps might cause significant voltage deviations and cable overloading, leading to reduced power quality and a violation of infrastructure constraints. The problem becomes even more critical when we consider that households often simultaneously consume a lot of power from the grid or simultaneously inject power back to the grid. The time that residents of households come back from work and start to charge their electric vehicles, and the presence of solar energy illustrate this correlation.

Another concern is that the mutual interdependence between the low-voltage grid and its supporting ICT network might reduce the reliability of the power grid [2], [3]. For example, a failure of a node in the ICT network might lead to inaccurate decisions about the power flows, which may result in voltage levels at some nodes of the low-voltage grid violating their operational boundaries. On the other hand, the failure of the power grid node(s) might in turn lead to failure of one or more nodes of the ICT network, and so on.

In this paper, we address the two major concerns mentioned above to improve the reliability of the future low-voltage grid. We focus both on improving the structure of the low-voltage grid itself, as well as identifying suitable levels of interdependency with the ICT network. To improve the structure of the low-voltage grid, we first study how its topological structure affects its operational performance. We use concepts from complex networks theory to characterize the topological structure of the low-voltage grid. Our operational performance indicators capture how well the node voltages and cable loads are maintained within their respective operational boundaries. Moreover, we propose relevant resiliency metrics to analyze the robustness of a low-voltage grid to attacks. Based on these findings, we propose a constraint programming formulation to optimize the critical structural features of a low-voltage grid at minimal cost. On top of that, we analyze the impact of the interdependence between the low-voltage grid and the communication network on the operational performance of the power grid under different scenarios and propose an algorithm to best deal with the dependency.

The remainder of this paper is organized as follows. In Section 2, related work is presented. Our structural assessment of the low-voltage grid is presented in Section 3, followed by our analysis of the interdependence between the power grid and ICT networks in Section 4. Concluding remarks are presented in Section 5.

2. Related work

In complex network analysis (CNA) real networks are represented by graphs and their dynamics are statistically analyzed to identify characterizing network features. Various such studies have been conducted on the power grid ([5] - [25]) following the major blackouts of America[2] and Italy[3] in 2003. The focus of these works include finding appropriate graph models to represent the power grid (e.g. [9], [11]), developing convenient graph metrics that characterize the power grid (e.g. [5], [6]), and analyzing the vulnerability of the power grid (e.g. [7], [14]). While most of them characterize the power grid in terms of classical topological metrics, such as the connectivity of the network, some of them employ topological metrics that reflect the electrical properties of the power grid.

Whereas most of the existing work on CNA of power grids focuses on the high-voltage grid, a recent work by Pagani and Aiello [6] presented a structural study of the medium-voltage and low-voltage grids, by identifying the influence of the topological structure of the grid on the cost of decentralized power trading.

Studies related to ICT networks for the power grid have also appeared. Fan et al. [26] described a typical ICT architecture for smart grids that is being reflected by the European standards development process as a hierarchical architecture consisting of home area networks (HAN), neighborhood area networks (NAN) and a wide area network (WAN). Niyato et al. [3] studied the reliability of smart grid wireless communications systems for demand-side management. Their analysis is based on a hierarchical system that consists of HANs, NANs and a WAN, where the nodes communicate using a wireless communication technology. There is a meter-data management system (MDMS) that performs the demand-side management in the WAN. To capture the reliability of the communications system, they map the availability of the wireless connection between nodes in the WAN to the cost of power-demand estimation error.

D'Agostino et al. [2] assessed methodologies that could be used to measure the interdependence between power grid and communication networks, namely topological, system theory based and simulation based approaches. Buldyrev et al. [27] presented a purely topological analysis of the interdependence between the high-voltage power grid and its supporting communication network. However, this study does not take the operational properties

[2] http://news.bbc.co.uk/2/hi/americas/3152451.stm
[3] http://news.bbc.co.uk/2/hi/3146136.stm

of the power grid into account.

Although the current trends indicate that the importance of the low-voltage grid is increasing, most of the work in the literature is focused on high-voltage grids, while the low-voltage grid seems to be largely ignored. In this paper, we attempt to fill this gap by taking the structural and operational properties of the low-voltage grid into consideration.

3. Structural assessment of the low-voltage grid

In this section, we assess the structure of the low-voltage grid with respect to its ability to cope with the dynamic load variations caused by the foreseeable demand and supply patterns.

3.1. Graph model of the low-voltage grid

A typical low-voltage grid, as shown in Fig. 1, is composed of an MV/LV transformer, strings of cables that are connected to the transformer, and end customers, such as households, each connected to the string cables through a tapping plug adapter. While in practice each string cable may contain three wires corresponding to three electrical phases, considering a single phase model is sufficient for the analysis in this work. In our graph model, the transformer and the tapping plug adapters are considered as nodes, while the segments of the strings of cables are the links. Moreover, we assume that the links are undirected since power flows bidirectionally in the cables as households can both consume and inject power.

Definition 1. *(Low-Voltage Grid Graph) A Low-Voltage Grid Graph having N nodes and L links is a graph $G(\mathcal{N}, \mathcal{L})$ where $\mathcal{N}$ and $\mathcal{L}$ denote the set of nodes and links, respectively, such that every node $n_i \in \mathcal{N}$ represents either a transformer or a tapping plug adapter that connects the end consumers to the low-voltage grid, and every link $l_{ij} \in \mathcal{L}$ represents the cable segment between the nodes n_i and n_j. The node that represents the transformer is denoted by n_t. Each link l_{ij} is associated with a weight Z_{ij} that represents the electrical impedance of the cable segment.*

Accordingly, our equivalent graph model of the radial low-voltage grid shown in Fig. 1 constitutes a path graph shown in Fig. 2. In addition to the path graph, we have generated different synthetic graphs that include instances of the common classes of graphs studied in the field of complex networks, namely the binary tree graph, Erdős–Rényi graph [28], scale-free graph [29], and small-world graph [30]. These graphs are generated mainly to obtain different types of theoretical graphs to undertake our studies.

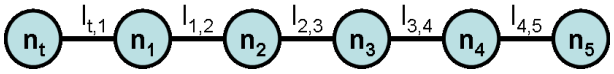

Figure 2: A path graph corresponding to a radial low-voltage grid.

A *rooted binary tree* is a graph with a tree structure in which each node has at most two child nodes. The *Erdős–Rényi graph* is a graph denoted by $G(N, p)$, where N is the number of nodes, and a link exists between any two nodes with probability p. A *scale-free graph* is a graph whose degree (i.e., the number of links connected to a node) distribution follows a power law, at least asymptotically. That is, the fraction $P(k)$ of nodes in the graph having k connections to other nodes is characterized by $P(k) = ck^{-\alpha}$ for large values of k, where c is a normalization constant and α is a parameter whose value is typically in the range $2 < \alpha < 3$. Scale-free graphs are characterized by presence of nodes, called hubs, that have degrees that greatly exceed the average degree of the network. Examples of real-life networks that exhibit the scale-free property are the world wide web, biological networks, and social networks. A *small-world graph* is a graph where the typical hop count d between two randomly chosen nodes (i.e., the number of steps required to traverse from one node to the other) grows logarithmically with the number of nodes N in the graph, i.e., $d \propto \log N$. Real-life networks, such as the food chain, network of brain neurons, and road maps, often exhibit the small-world property.

3.2. Structural metrics

In this section, we present both generic metrics that are used in complex network analysis, as well as metrics that are specific to the low-voltage grid to capture the structural properties of the low-voltage grid. Although there is a rich set of complex network metrics [31], not all are applicable, for instance due to the different robustness properties of the low-voltage grid as will be explained in Section 3.6. We therefore select generic metrics that seem most relevant for the structural properties of the low-voltage grid, namely *average path length, eccentricity*, and *clustering coefficient*.

In the low-voltage grid, the MV/LV transformer plays a special role. The voltage level at the transformer remains stable, while substantial voltage variation might occur at the nodes further from the transformer depending on the power flow patterns in the grid. Thus, it is advantageous for a node to be connected closer to the transformer. Moreover, if a node loses connection to the transformer, it loses the stability provided from the strong

back-bone power grid. Accordingly, we define three low-voltage grid related metrics, namely *closeness to transformer, link betweenness to transformer*, and *net-ability to transformer*.

3.2.1. Average path length (γ)

The average path length of a graph characterizes the distance traveled on average to connect any two nodes in the graph. For a given graph G, the average path length, γ, is defined as the average of the shortest path lengths in terms of hop count between all pairs of nodes in the graph.

3.2.2. Eccentricity (ε)

For a node n_i in a graph G, the eccentricity ε_i is defined as the distance of the longest path among all the shortest paths between the node n_i and all the other nodes in G. We employ the *transformer eccentricity*, ε_t, to measure the distance of the most distant node from the transformer, because the transformer plays a special role in the low-voltage grid.

3.2.3. Clustering coefficient (C)

The clustering coefficient of a node in a graph measures how densely connected its neighbors are to each other. Let k_i denote the number of neighbors of a node n_i, and let q_i denote the number of links between its neighbors. Then, the clustering coefficient C_i of the node n_i is obtained as:

$$C_i = \frac{2q_i}{k_i(k_i - 1)} \tag{1}$$

where $k_i(k_i - 1)/2$ represents the maximum number of links between k_i nodes. The clustering coefficient of the whole graph, C, is the average node clustering coefficient over all the nodes in the graph.

3.2.4. Closeness to transformer (θ)

Closeness to transformer captures how closely connected the nodes are to the transformer. We derive the closeness, θ_i, of a node n_i to the transformer node n_t from the electrical distance between them, which is expressed in terms of the equivalent impedance between them, Z_{it}. The equivalent impedance between nodes n_t and n_i can be obtained as follows. We inject a unit current I_{unit} at n_t and absorb the same amount at n_i, while all the other nodes neither inject nor absorb current. Then, the equivalent impedance Z_{it} is obtained as shown in Eq. 2, where v_t and v_i denote the voltage levels at nodes n_t and n_i, respectively.

$$\frac{1}{\theta_i} = Z_{it} = \frac{(v_t - v_i)}{I_{unit}} = v_t - v_i \tag{2}$$

We define the closeness to the transformer, θ_i, of a node n_i ($n_i \neq n_t$) as the inverse of the equivalent impedance between n_i and n_t. The closeness to transformer of the entire network, θ, is given in Eq. 3, where the first term represents the average closeness of the nodes to the transformer, whereas the second term, which is a function of the standard deviation, captures how evenly the θ_i's are distributed. Ideally, each node has large closeness value and the closeness of all the nodes are fairly distributed.

$$\theta = \mu_\theta \times \frac{1}{1 + \sqrt{\frac{1}{N-1}\sum_{i \in \{1,..,N\} \setminus \{t\}} (\theta_i - \mu_\theta)^2}} \tag{3}$$

3.2.5. Link betweenness to transformer (β)

Link betweenness to transformer is a measure that expresses how strategically located a link is to support the electricity flow between the transformer and the other nodes in the low-voltage grid. In this work, we adopt a suitable definition of link betweenness for power systems proposed in [5] with a modification to reflect the unique property of the low-voltage grid. While in [5] link betweenness is computed using electricity flows between all pairs of nodes in the high-voltage network, we compute the link betweenness to transformer using the electricity flows between the transformer node, n_t, and all the other nodes of the network. To do so, we inject a unit current from n_t and absorb it at n_i, while the other nodes neither inject nor absorb current. We denote the portion of the injected current that flows through link l_{jk} by $f_{l_{jk}}^{it}$. This is repeated for every other node $n_i \neq n_t$. The link betweenness to transformer of a link l_{jk} is then given in Eq. 4. β_{jk} represents the betweenness of the link l_{jk} in terms of the amount of current that flows through the link when current flows between the nodes and the transformer, weighted by the total flow.

$$\beta_{jk} = \frac{\sum_{i \in \{1,..,N\} \setminus \{t\}} f_{l_{jk}}^{it}}{N-1} \tag{4}$$

The link betweenness of the entire network is given in Eq. 5, where μ_β is the average of the betweeness of the links. Ideally, the betweenness of the links are small (the first term), because a large value of β_{jk} means that the link l_{jk} has good chance of being overloaded, and the betweenness levels of

the links are fairly distributed (the second term).

$$\beta = \frac{1}{\mu_\beta} \times \frac{1}{1 + \sqrt{\frac{1}{L}\sum_{l_{jk}\in\mathcal{L}}(\beta_{jk} - \mu_\beta)^2}} \tag{5}$$

3.2.6. Net-ability to transformer (η)

Net-ability to transformer measures the electrical transmission capacity of the network per the electrical impedance it presents to the electricity flow. Net-ability has been proposed in [5]. We adopt this with a modification to reflect the unique property of the low-voltage grid. We compute the net-ability to transformer using the electricity flows between the transformer node, n_t, and all the other nodes of the network.

We reuse $f^{it}_{l_{jk}}$ that was computed previously. Let $P^{\max}_{jk}$ denote the line flow limit of the link l_{jk}. The maximum amount of current that can be injected at n_t and absorbed at n_i without exceeding the maximum current flow capacity of link l_{jk} is given by $I^{\max}_{jk}/f^{it}_{l_{jk}}$. Thus, the maximum current that can be injected, ϕ_{it}, is limited by the link that reaches its flow capacity the earliest as given in Eq. 6.

$$\phi_{it} = \min\{\frac{I^{\max}_{jk}}{f^{it}_{l_{jk}}}, \text{ where } l_{jk} \in \mathcal{L}\} \tag{6}$$

The net-ability to transformer of the entire network is obtained as shown in Eq. 7. By incorporating both the maximum flow capacity and the impedance between the transformer and the other nodes, η effectively measures the efficiency of the network.

$$\eta = \frac{1}{N-1} \sum_{i\in\{1,..,N\}\setminus\{t\}} \frac{\phi_{it}}{Z_{it}} \tag{7}$$

3.3. The operational performance metrics

As discussed in Section 1, managing the node voltages and the link loads are major challenges in a prosumer-dominated low-voltage grid. Hence, it is important to examine the number of nodes and links whose voltage levels and load levels, respectively, are within the acceptable boundaries, when subject to a certain load scenario. Accordingly, our operational performance metrics attempt to capture how well the node voltage levels and the cable loads are maintained within their corresponding acceptable boundaries. Given a certain load profile of the households connected to the low-voltage grid, let x be the number of nodes whose voltage levels lie in the acceptable operational

boundaries, and y be the number of links whose loads lie in the acceptable operational boundaries under the applied load profiles. Then, we define two operational performance measures, namely, the voltage feasibility ratio $R_{voltage}$ and the load feasibility ratio R_{load} as:

$$R_{voltage} = \frac{x}{N} \tag{8}$$

$$R_{load} = \frac{y}{L} \tag{9}$$

These performance metrics are relevant, because the larger $R_{voltage}$ and R_{load} are, the more nodes and links remain within their corresponding operational boundaries, and hence the better the performance of the low-voltage grid.

3.4. Simulation set-up

We simulate the electrical dynamics of the low-voltage grid using a low-voltage network simulator named Gaia [32], which is commonly used by network operator companies in The Netherlands, such as Alliander[4]. While Gaia has various functionalities, for this study, we are interested in its load flow analysis functionality. Using Gaia, we construct different low-voltage grids corresponding to instances of radial (RA), binary tree (BT), Erdős–Rényi (ER) random, scale-free (SF), and small-world (SW) networks and observe the voltage levels and the cable loads under various load scenarios.

The transformer and cable parameter specifications used in our simulations are constructed from data obtained from Alliander. After analyzing the rich set of data about their low-voltage grid network specifications, we chose the most representative parameter specifications. Namely, the $400V$, $630KVA$ transformer and the $50mm^2$ copper cable are used. Our candidate networks are set to have equal number of nodes and comparable number of links to reach a fair comparison among them. We generated the random, small-world, and scale-free networks using the *igraph* library[5] of the *R network visualization tool*, by trying to stay close to the size of the radial network. While each network has $N = 50$ nodes, the number of links are 50, 50, 54, 50, and 53, respectively, for the radial, binary tree, random, scale-free and small-world networks. The plots of the random, scale-free and small-world networks are shown in Fig. 3, Fig. 4, and Fig. 5, respectively. The nodes with a red color represent the transformer nodes (n_t). In each

[4]Alliander is a distribution network operator in The Netherlands owning 40% of the distribution networks.

[5]http://igraph.sourceforge.net

network, the node that yields the minimum average shortest distance to all the other nodes in the network was selected as n_t.

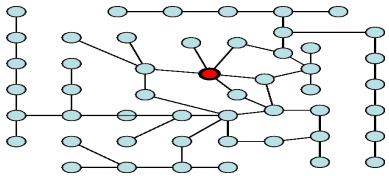

Figure 3: The Erdős–Rényi random network.

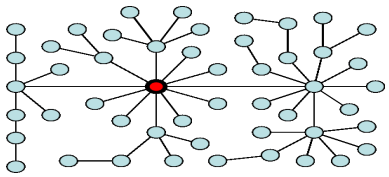

Figure 4: The scale-free network.

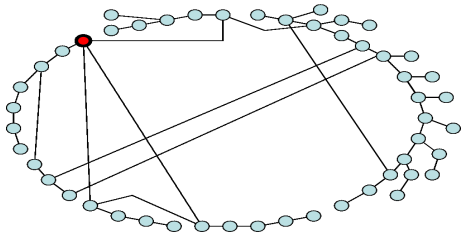

Figure 5: The small-world network.

We consider three different scenarios for the load patterns. The first scenario (*S1*) is based on a classical household load profile. The second scenario (*S2*) is a futuristic scenario where each household has an electric vehicle, a solar panel and a micro-CHP in addition to the classical load profile. The electric vehicles are charged immediately after the driver comes home; where the patterns of the time at which the drivers arrive at home are derived from a 2009 mobility research in The Netherlands [33]. The data representing the classical household load and production of solar panels and micro-CHPs were obtained from Alliander, which are meter measurements taken every 15 minutes for a period of 24 hours (96 readings). Load scenarios S1 and S2 each have 96 different loading conditions corresponding to the 96 measurements taken every 15 minutes during 24 hours. Fig. 6 shows the

components of the scenarios S1 and S2 load profiles of a household. To make different profiles for each household, we randomized the values using Monte Carlo method. Thirdly, we have a synthetic worst-case scenario (*S3*) where the households have the same loads. In S3, we start from a small value for the loads of the households and gradually increase them in steps.

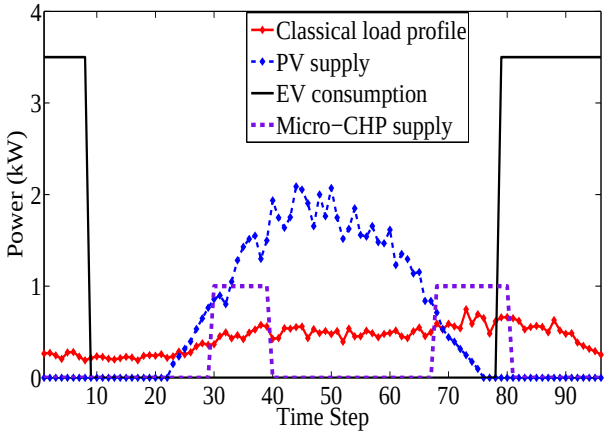

Figure 6: The components of the household load profiles.

3.5. Analysis of the networks

In this section, the structural and operational metrics of the candidate networks are presented together with their correlations. A summary of the values of the structural metrics for the candidate networks is shown in Table 1. Although the networks are instances of different classes of networks, our aim is not to study the features of the different classes of networks, nor do we claim that these networks are typical representatives of their respective network classes. The names of the network classes are used as labels of our networks for better readability.

The very low values of the clustering coefficient (C) result from the fact that the ratio of number of links to number of nodes ($\frac{L}{N}$) is one or very close to one for all our networks. Only the SW network has an instance where neighbors of a node are also connected to themselves, hence a non-zero value of C. As depicted by the average path length (γ), in the radial network the longest distance is traveled to connect any two nodes that are picked at random. Whereas, in the scale-free network, presence of the hub nodes reduces the distance traveled to connect any two nodes in the network.

Table 1: Summary of the values of the structural metrics corresponding to the candidate networks (RA = radial, BT= binary tree, ER = Erdos–Rényi, SF = scale-free, SW = small world).

	RA	BT	ER	SF	SW
C	0	0	0	0	0.017
γ	17	6.09	6.234	3.709	6.007
ε_t	25	5	9	4	10
θ	0.7	1.548	1.256	1.813	1.238
η	40.407	76.33	122.663	145.121	105.8748
β	3.42	47.698	9.936	21.67	8.869

The radial network has the worst values for each of the low-voltage specific structural metrics. The low values of its closeness (θ) and net-ability (η) metrics, as well as the large transformer eccentricity ε_t stem from the large electrical distance most of the nodes have from the transformer. On the other hand, the scale-free network has the highest closeness and net-ability metrics, and the lowest ε_t, since most of its nodes are located at short electrical distance from the transformer. In terms of the link betweenness to transformer (β), the binary tree network yields the best value, which stems from two reasons. First, most of the links are adjacent to the leaf nodes of the binary tree, and such links experience only a small amount of current flow corresponding to the leaf node, thereby yielding a small value of μ_β in Eq. 5. Second, the links on the same level of the binary tree experience a similar amount of load, giving rise to a small value of the standard deviation term in Eq. 5. The Erdős–Rényi and the small-world networks have moderate metric values, while the Erdős–Rényi network yields better values for most of the metrics. In general, the candidate networks have different structural properties.

We have summarized the operational performance of our five candidate networks under different loading scenarios in Table 2. For the load scenarios S1 and S2, each value of $R_{voltage}$ and R_{load} in the table is an average of 96 values representing the corresponding values for the 96 time steps, while each value shown for S3 represents an average over seven corresponding values that are obtained by assigning loads of $1, 2, .., 7$ kW at each household. Under scenario S1, for all candidate networks, all the node voltage and cable load levels remain within the acceptable operational boundaries. Although the radial network was doing well with the conventional load scenario S1, the results under S2 reveal its insufficiency to support the future load scenario. Moreover, the classical radial network yields the lowest performance under

Table 2: Summary of the operational performance of the candidate networks.

		RA	BT	ER	SF	SW
S1	$R_{voltage}$	1	1	1	1	1
	R_{load}	1	1	1	1	1
S2	$R_{voltage}$	0.74	1	1	1	1
	R_{load}	0.68	0.94	0.96	0.98	0.94
S3	$R_{voltage}$	0.257	0.597	0.71	0.846	0.64
	R_{load}	0.466	0.89	0.88	0.946	0.868

Table 3: Correlation of the structural and operational metrics.

	θ	η	β	C	γ	ε_t
$R_{voltage}$	0.77	0.81	0.27	0.03	-0.8	-0.77
R_{load}	0.88	0.83	0.48	0.16	-0.99	-0.97

S3 compared to the other networks. This clearly indicates that the radial topological structure that is being widely used in the low-voltage grid is not capable of supporting the future load profiles.

The difference in the operational performances of the candidate networks is influenced by the differences in their structural properties. To reveal this, we measure the correlation of the structural metrics listed in Table 1 against the values of the operational metrics, $R_{voltage}$ and R_{load}, that are obtained under the different simulation scenarios. We use the Pearson's correlation coefficient. Clearly, $R_{voltage}$ and R_{load} do not show any correlation with the structural metrics in the cases when $R_{voltage} = 1$ and $R_{load} = 1$ for all the networks. Apart from these special cases, Table 3 presents the summary of the correlations averaged over the different scenarios.

Our findings suggest that there are strong correlations between operational performances of the low-voltage grid and some of its structural properties. For example, the voltage feasibility ratio ($R_{voltage}$) shows strong correlation with the structural metrics θ, η, γ and ε_t. Accordingly, if a network operator wants to improve the feasibility ratio of its network, (s)he needs to focus on modifying the structural aspects of the low-voltage grid that improve θ, η, γ and ε_t.

3.6. Resilience to link failure

The links in a low-voltage grid may fail due to aging, overloading, or by intentional attacks. In a low-voltage grid, a fuse is connected at the beginning of every cable that is connected to the transformer. The portion

of the low-voltage network that is connected to the transformer through a fuse forms a sub-network of the low-voltage network. In Fig. 7(a), if the link between H2 and H3 fails, then F1 burns, thereby disconnecting sub-network1 from the transformer. While in general networks adding a link improves network reliability [34], when the two sub-networks are coupled by a link as in Fig. 7(b), failure of the link burns both fuses F1 and F2, disconnecting all the houses from the transformer.

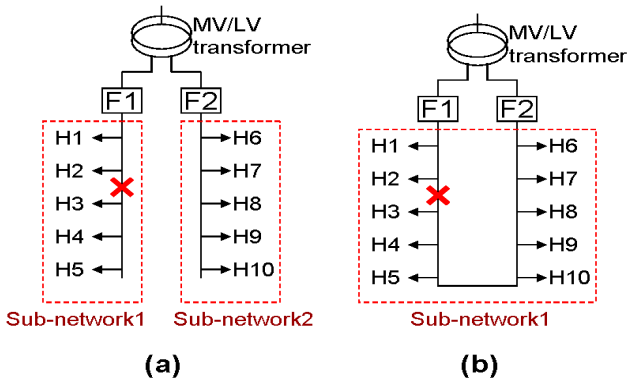

Figure 7: Example of two networks to describe the effect of adding a bridge link between sub-networks.

Let M be the number of sub-networks of the low-voltage grid that do not have a link that couples them. If there are two or more sub-networks that have link bridges between them, then they are represented by one bigger sub-network that is the union of the individual sub-networks. Let us denote the number of nodes in the sub-network that contains the link l_{ij} ($l_{ij} \in \mathcal{L}$) by N_m. Clearly, N_m represents the number of nodes affected by the failure of l_{ij}. Hence, the resilience ϕ_{ij} of the low-voltage grid to failure of the link l_{ij} is given in Eq. 10. Thus, the average resilience of the low-voltage grid to a single link failure, ϕ_{avr}, can be obtained by averaging ϕ_{ij} over all the links $l_{ij} \in \mathcal{L}$. Our candidate networks BT, RA, ER, SF and SW have yielded ϕ_{avr} values of 0.5, 0.5, 0.0385, 0.745 and 0.305, respectively. The SF network yielded large ϕ_{avr} value since it has many sub-networks of the low-voltage network that do not have link coupling between them, hence only a small part of the network is affected by a single link failure.

$$\phi_{ij} = 1 - \frac{N_m}{N} \tag{10}$$

When, a sequential failure of multiple links occurs, the resilience of the

low-voltage grid after the failure of the i^{th} link can be obtained as shown in Eq. 11, where N_m^j is the number of nodes affected when the j^{th} link fails.

$$\phi^i = 1 - \sum_{j=1}^{i} \frac{N_m^j}{N} \tag{11}$$

To better analyze the resilience of the low-voltage network to sequential failure of multiple links, we employ the *envelop of perturbation* that was introduced in [35]. Let $\phi^i_{\max}$ be the resilience of the low-voltage grid after the failure of the i^{th} link if the link that affects the *smallest* number of nodes fails in each step, and let $\phi^i_{\min}$ be the corresponding resilience of the low-voltage grid if the link that affects the *largest* number of nodes fails in each step. The area between $\phi^i_{\max}$ and $\phi^i_{\min}$, called the envelop of perturbation, quantifies the uncertainty of the amount of risk of link failure. Moreover, a graph G_1 is more resilient than graph G_2 if $\phi^i_{\min}(G_1) > \phi^i_{\max}(G_2)$, for all i^{th} link failures.

Under consecutive link failures, the SF network outlives the failures compared to the other four networks owing to its larger number of sub-networks that do not have link couplings, whereas the other networks completely fail after consecutive failure of two links, since they have only two decoupled sub-networks. Fig. 8 shows that the envelop of the SF network lies above that of the ER network in most of the cases, but not entirely. Hence, we cannot conclude that the SF network is always more resilient than the ER network. Similar plots have shown that the SF network was always more resilient than the RA and BT networks.

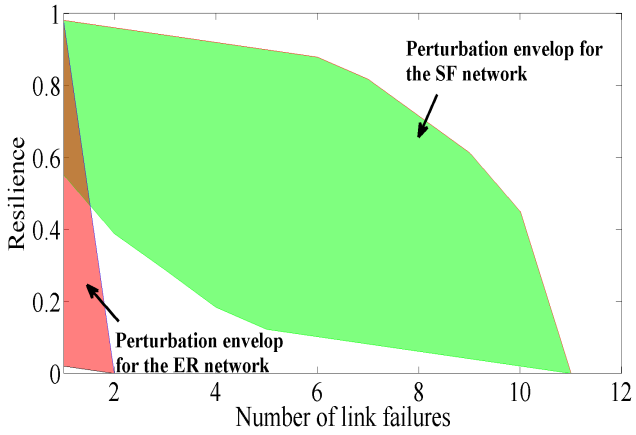

Figure 8: The perturbation envelops for two networks.

In conclusion, the results reveal that the resilience of a low-voltage network to link failures increases if there are more sub-networks that are not coupled by links. Hence, paradoxically, inserting links to couple the sub-networks reduces its resilience. Moreover, the size of the sub-networks, in terms of the number of nodes, influences the resilience of the network to link failures.

3.7. Low-voltage network design

In this section, we investigate how to design a low-voltage network that delivers a required level of performance with optimal cost. To this end, we attempt to design the low-voltage network such that the influential structural metrics are improved by specific amounts, while the cost of doing so is minimized. In our case, the cost is expressed in terms of the total length of cables used. The influential structural metrics are strongly dependent on the distance of the nodes from the transformer, thus, our design aims at guaranteeing a required bound on the average distance of the nodes from the transformer. In our design, we avoid coupling links between sub-networks that are connected to different fuses to increase the resilience to link failures.

The design problem has two sub-parts:

1. Finding the best location for the transformer, and
2. determining the placement of the links in the low-voltage grid.

For optimal transformer placement, we first construct a complete graph with links between each pair of nodes, where the nodes are the tapping plug adapters that connect the houses to the low-voltage grid (as described in Definition 1), and each link has a weight that corresponds to link distance. After computing the shortest distance from each node to every other node in the graph, we select the node with the minimum average distance to all the nodes, and select it as transformer node, because we want to minimize the average distance of the nodes from the transformer. While this transformer placement strategy minimizes its distance to all other nodes, a different transformer placement strategy can still be employed without affecting our solution for the second part of the problem.

Once the placement of the transformer is determined, the second part of the problem is determining the cost-optimal placement of the links (cables) in the low-voltage grid such that the average distance of the nodes from the transformer is below a given bound. We propose a constraint programming formulation to solve this problem.

The following notation is used in our formulation:

- $\mathcal{N}$: The set of indices of nodes in the LV network, $\mathcal{N} = \{1, 2, ..., N\}$.
- $E_{i,j}$: Predefined constant. Represents the length of a cable required to establish a direct link between the nodes n_i and n_j. If it is not possible to insert a direct link between the nodes n_i and n_j, then $E_{i,j}$ is set to ∞.
- $H_{i,j}$: A binary variable that equals 1 if a link is placed between the nodes n_i and n_j, and 0 otherwise.
- $\mathbf{K}$: a set of stages involved to compute the shortest distances, $\mathbf{K} = \{1, 2, ..., N\}$.
- $D_{i,k}$: The shortest distance from n_i to n_t (the transformer node) at stage k. $D_{i,N}$ represents the actual shortest distance from n_i to n_t.
- $S_{i,k}$: A binary variable that is equal to 1 if node n_i is in the visited list at stage k.
- M_k : The minimum distance from the transformer among the nodes that are not yet in the visited list at stage k.
- A_k: The index of the node added to the visited list at stage k.
- D^*: The average distance of the nodes from the node where the transformer is connected, n_t.
- Δ: Predefined constant. The maximum allowed average distance from n_t.

The variable H, which indicates whether a link is placed between a pair of nodes, can take only boolean values (Eq. 12). Since power can flow in both directions in each cable of the LV Grid, the links are undirectional (Eq. 13).

$$H_{i,j} = \{0, 1\}, \quad i, j \in \mathcal{N} \tag{12}$$

$$H_{i,j} = H_{j,i}, \quad i, j \in \mathcal{N} \tag{13}$$

The constraints in Eq. 14 - 24 are used to compute the shortest distances from each node to the transformer. This computation involves a set of iterative stages, $k \in \mathbf{K}$. Eq. 16 - Eq. 18 set the values of the variables for the first iteration stage. The variable $S_{i,k}$ is set to assume only binary values in Eq. 14, indicating that a node n_i can either be in the visited set or not at

any iteration stage k. The distance of the transformer node to itself is set to zero (Eq. 15), while the distances of the other nodes to the transformer are initialized to infinity (Eq. 16).

$$S_{i,k} = \{0,1\}, \quad i \in \mathcal{N}, k \in \mathbf{K} \tag{14}$$

$$D_{t,1} = 0 \tag{15}$$

$$D_{i,1} = \infty, \, i \in \mathcal{N} \backslash \{t\} \tag{16}$$

So far, the visited set is empty, that is, all the nodes are unvisited. At each iteration stage, the node with the shortest distance to the transformer among the unvisited ones is added to the visited set. Then, the shortest distance so far from the unvisited nodes to the transformer is identified to be 0 (Eq. 17). Afterwards, the particular node with the shortest distance, which in this case is the transformer node itself, is identified as the node that is to be added to the visited set at the current iteration stage (Eq. 18). Then, the visited set is updated by adding the transformer node to the set (Eq. 19) and leaving the other nodes unvisited (Eq. 20).

$$M_1 = 0 \tag{17}$$

$$A_1 = t \tag{18}$$

$$S_{t,1} = 1 \tag{19}$$

$$S_{i,1} = 0, \, i \in \mathcal{N} \backslash \{t\} \tag{20}$$

The values of the variables for stages $k = 2, ..., N$ are computed in Eq. 21 - 24. The distance of each of the nodes from the transformer node at stage k is computed in Eq. 21. The equation has three terms that are in square brackets. The distance of the node at the current stage is set to its distance in the immediate-lower stage if either of the following two cases hold. The first case is if n_i is in the visited set at the immediate-lower stage (the first term). The second case is if n_i is not in the visited set at the immediate-lower stage and if at the same time a direct link is not placed between itself and the node added to the visited list at the immediate-lower stage, $n_{A_{k-1}}$ (the second term). However, if n_i is not in the visited set at the immediate-lower stage and if a link is placed between itself and the node added to the visited set at the immediate-lower stage, $n_{A_{k-1}}$ (the third term), then its distance at stage k is equated to the minimum value among its distance at the immediate-lower stage and the sum of the length of the direct link between n_i and $n_{A_{k-1}}$ and the distance of $n_{A_{k-1}}$ at the immediate-lower stage.

$$
\begin{aligned}
D_{i,k} \;=\; & [S_{i,k-1} \times D_{i,k-1}] + [(1 - S_{i,k-1}) \times (1 - H_{i,A_{k-1}}) \times D_{i,k-1}] + \\
& [(1 - S_{i,k-1}) \times H_{i,A_{k-1}} \times \min(D_{i,k-1}, E_{i,A_{k-1}} + D_{A_{k-1},k-1})], \\
& k \in \mathbf{K}\backslash\{1\}, i \in \mathcal{N} \qquad (21)
\end{aligned}
$$

Eq. 22 computes the minimum distance among the distances of the nodes that are not in the visited set in the immediate-lower stage, and Eq. 23 assigns the index of the node with the minimum distance computed in Eq. 22 as the node that is added to the visited set at stage k. The max operator is used to select one node with the larger index when there is a tie. The term $(M_k == D_{i,k-1})$ is a conditional expression that takes a value of 1 if M_k is equal to $D_{i,k-1}$, or 0 otherwise. In Eq. 24, the $S_{i,k}$ of the nodes at stage k are updated, where the value is set to 1 for the node that is added to the visited set at the current stage, while for the other nodes $S_{i,k}$ is set to $S_{i,k-1}$.

$$
\begin{aligned}
M_k \;=\; & \min_i(\infty \times S_{i,k-1} + D_{i,k}), \quad k \in \mathbf{K}\backslash\{1\}, i \in \mathcal{N} && (22) \\
A_k \;=\; & \max_i(i \times (1 - S_{i,k-1}) \times (M_k == D_{i,k-1})), \\
& k \in \mathbf{K}\backslash\{1\}, i \in \mathcal{N} && (23) \\
S_{i,k} \;=\; & (i == A_k) \times 1 + (i \neq A_k) \times S_{i,k-1} && (24)
\end{aligned}
$$

Eventually, $D_{i,N}$ represents the actual shortest distance of node n_i from the transformer. The average distance of the nodes from the transformer (D^*) is computed in Eq. 25, and Eq. 26 makes sure that the average distance is below the upper bound, Δ. In Eq. 27, the total cost of the links in the network is computed as the sum of the costs of the individual links.

$$
\begin{aligned}
D^* \;=\; & \frac{1}{N} \sum_i D_{i,N}, \quad i \in \mathcal{N} && (25) \\
D^* \;\leq\; & \Delta && (26) \\
cost \;=\; & \frac{1}{2}\Big(\sum_{i,j \in \mathcal{N}} E_{i,j} \times H_{i,j}\Big) && (27)
\end{aligned}
$$

The total cost is minimized in the CP model, as follows:

$$
\begin{aligned}
& \textbf{minimize } cost && (28) \\
& \textbf{subject to } \text{Eq. } 12 - \text{Eq. } 27.
\end{aligned}
$$

Table 4: Comparison of the cost of the five different low-voltage grid topological structure designs.

D^*	82	75	70	65	60
$Cost$	1 800	1 824	1 848	2 064	2 384

We implemented our constraint programming formulation and solved it using the ILOG solver. We have applied our low-voltage grid topological structure design strategy to a hypothetical neighborhood that is composed of $N = 120$ houses arranged in a rectangular lattice structure of 10×12 nodes. We assume that the distances between consecutive nodes across all the rows and columns are each 15 m. Fig. 9 shows the comparison of the performance of five different cost-optimal low-voltage networks designed for the same neighborhood with different bounds on the average distance from the transformer. As can be observed from Fig. 9, the operational performance of the network is higher for lower values of the average distance from the transformer (Δ). This arises from the strong dependence of the influential structural metrics on D^*, whereby lower D^* leads to more suitable values of the influential structural metrics, thereby boosting the operational performance. However, the performance improvement comes at the cost of using more cables, as is revealed in Table 4.

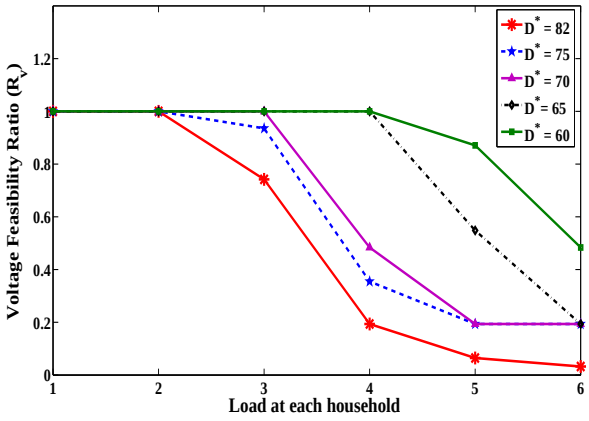

Figure 9: Comparison of the performance of LV grid designs in terms of the voltage feasibility ratio.

Our proposed design algorithm can be readily applied to design a low-voltage grid for a new neighborhood. It can also be applied to redesign an

existing low-voltage grid.

So far in this study, we have dealt solely with the structure of the low-voltage grid to increase its reliability. But, making the structure of the low-voltage grid robust is not enough by itself to conveniently support the load dynamics. The power output from renewable sources, such as solar panels, might frequently vary with the weather conditions. Moreover, the energy consumption patterns of the households could show rapid variations due to the unpredictable behaviors of the residents of the houses. As a result, the load profiles of the households become more unpredictable, which requires enhancing the intelligence of the low-voltage grid to cope. It is commonly understood that intelligence of the future smart grid is supplied through the support of ICT networks. While the low-voltage grid relies on ICT networks for its intelligence, the nodes of the ICT network might at the same time depend on the low-voltage grid itself for power supply. This bidirectional interdependence between the two networks also poses challenges on the reliability of the low-voltage grid, which will be studied in the following section.

4. Interdependence between the low-voltage grid and ICT networks

A node in the ICT network supporting the power grid may either totally depend on the power grid for its power supply, or can have optional backup power supply, such as uninterrupted power supply (UPS). If the ICT node does not have a backup power supply, then it fails when the grid node that supplies its power fails. Whereas the ICT node can continue to function after its power-supplying grid node fails if it has a backup power supply. However, installing a backup power supply for each ICT node increases the cost of the ICT network. Thus, a network designer might allow some ICT nodes to depend on the power grid to reduce cost.

The interdependence between the power grid and its supporting ICT network raises concerns about the reliability of the power grid. Thus, it is essential to assess how their interdependence affects the reliability of the grid.

For this study, we consider a neighborhood energy community that is composed of prosumer households that are connected to a low-voltage grid. There is an energy community agent (aggregator) that coordinates the load profiles in the neighborhood energy community, as well as trades power with the rest of the grid representing the energy community [36]. The coordination involves information exchanges that take place over an ICT network.

In practice, ICT networks are not yet deployed at the low-voltage grids. However, possible ICT network architectures for the power grid are being proposed in the scientific literature. In this work, the ICT network is formed from a hierarchy of networks as is a common practice in the related literature [26], [3], [37]. We consider a generic network with three hierarchical levels [3]: Home-Area Networks (HANs), information Relay Nodes (RN), and Meter-Data Management System (MDMS). The HAN is the ICT layer that interconnects the smart appliances in the home with the smart meter and the home gateway. The home gateways exchange information between the smart meter and the information relay node in the micro-neighborhood. The information relay nodes of the micro-neighborhoods form a network and relay information between the HANs and the MDMS. The information relay nodes could represent switches in wired communication networks or relay stations of a wireless network. The MDMS manages the information gathered from the houses and computes the required control variables. The MDMS is located at the energy community agent. Fig. 10 depicts the ICT network architecture. The ICT nodes, such as the home gateways and the RN, can either fully depend on the grid power supply from the household or may have a backup power supply that allows them to keep communicating with the MDMS if the supplying grid node fails.

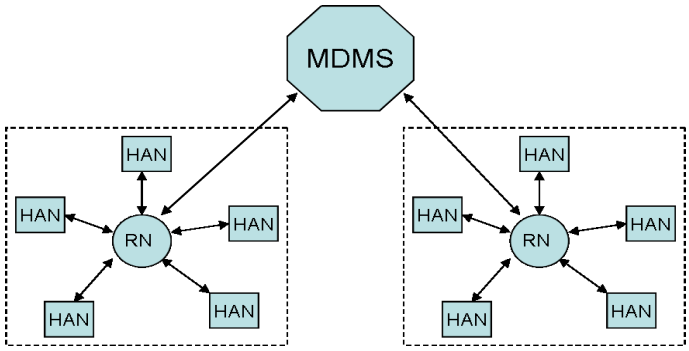

Figure 10: The architecture of the communication network.

If an ICT node fails, the information about the corresponding grid node (for home gateway node) or set of grid nodes (for information relay node) cannot reach the MDMS. Hence, the MDMS allocates loads by making assumptions about these nodes whose information is missing. If the actual loads at these grid nodes deviate from the assumed load levels, then the allocation of MDMS becomes erroneous. These uninformed allocations might result in a load flow pattern in the low-voltage grid that leads to over/under

voltages at some grid nodes. Normally, tap changing transformers are used to control the voltage level at the transformer so that the voltage levels at the other nodes remain within operational boundary. The taps of such transformers are changed manually, which might take a long time. The output voltage of some modern transformers can be controlled using automatic transformer tapping technologies, which could help to control the over/under voltages. However, this technology is not deployed in low-voltage grids. Thus, the grid nodes that experience under/over voltage before the technician reaches the transformer will fail and will be disconnected from the grid. Accordingly, we measure the performance of the low-voltage grid by the voltage feasibility ratio that was defined in Eq. 8.

4.1. Simulation setup

For this simulation, we employ a low-voltage grid with the classical radial structure shown in Fig. 1, and we adopt the $400V$, $630KVA$ transformer and the 50 mm^2 copper cable for our simulations. Simulations are also conducted with the other low-voltage grid topologies that were used in Section 3, namely, the radial, binary-tree, scale-free, small-world and random networks.

We employ the ICT network architecture shown in Fig. 10. We consider different scenarios of the dependence of the ICT nodes on the power grid for their power supply:

1. independent scenario (S_{indep}): all the ICT nodes have backup power supply,
2. fully dependent scenario (S_{full_Dep}): no ICT node has backup power supply, and
3. partial dependence scenario ($S_{partial\_Dep}$): only the information relay nodes have backup power supply, while the home gateways do not have one.

The coordination strategy in the energy community is assumed as follows. There is an expected load pattern of each household during the day based on the day-ahead agreement between the houses and the aggregator. Each day is divided into a fixed number of time steps. At the beginning of each time step, each household sends to the aggregator: (1) its planned load for the time step and (2) the possible flexibility $\pm x\%$ in the reported load. Then, the aggregator assigns the operational load for the current time step to each household within the reported flexibility ranges so that the aggregate load of the entire community is as close as possible to the expected aggregate load in the day-ahead agreement. If the MDMS does not receive

any information from an ICT node at a time step, it assumes that the load at the corresponding grid node is the same as the expected load reported in the day-ahead profile and allocates the loads accordingly.

We consider the impact of ICT node failure and grid node failure separately. For each case, we introduce a node failure and observe how its effect propagates in the two networks under the three interdependence scenarios described before. When the ICT node fails, at the corresponding grid node, we introduce a load that has large difference from the day-ahead load profile to represent a possible situation where the actual load significantly deviates from the expected load.

The power flow in the low-voltage grid is simulated using the Gaia software that was introduced in section 3.4. The interdependence between the two networks is captured using a Matlab function that is interfaced with Gaia.

4.2. Simulation results

In Section 1, we have argued that a failure of a node can lead to a reverberating failure of nodes in both networks. Fig. 11 shows such a result where a failure of an ICT node at a household, in a scenario where all the ICT nodes depend on the power grid, leads to cascading failures thereby deteriorating the performance of the radial low-voltage grid across time steps. In the first time step, we introduced failure of an ICT node, and assigned a load that deviates from its expected day-ahead value at the corresponding grid node. The power flows resulting from this uninformed load allocation resulted in failure of some grid nodes, hence the feasibility ratio lower than 1 in the first time step. The corresponding ICT nodes of these failing grid nodes also failed, hence the information about the failure of the grid nodes cannot be reported to the MDMS in the second time step. Hence, the MDMS makes another uninformed operational load allocation in the second time step, and so on, leading to the cascading failures shown in the figure.

During our simulations, similar cascaded failures have been observed with the other low-voltage grid topologies. In the remainder of this section, we therefore only present our results on the interdependence between the classical radial low-voltage grid and its supporting ICT network.

Fig. 12 depicts a result of the voltage feasibility ratio ($R_{voltage}$) averaged over time steps for the interdependence scenarios S_{full_Dep}, $S_{partial\_Dep}$, and S_{indep}, in response to a failure of a grid node representing a household. As can be observed, in both S_{full_Dep} and $S_{partial\_Dep}$, the voltage feasibility performance of the power grid has deteriorated compared to its corresponding

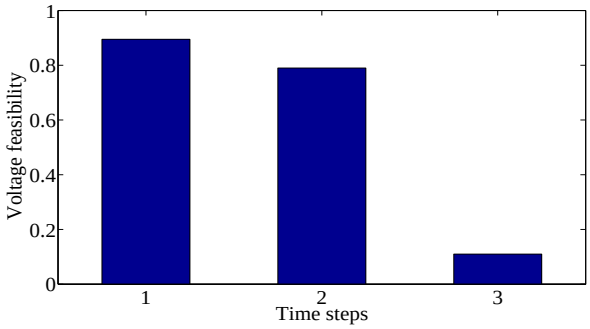

Figure 11: Performance of the power grid in response to a failure of an ICT node at a household.

performance in S_{indep}. Further, $S_{partial\_Dep}$ yields better grid performance compared to S_{full_Dep}. A fairly similar result is obtained for the interdependence effect in response to a failure of the ICT node of a household.

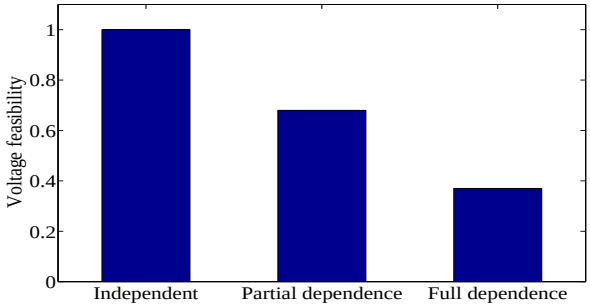

Figure 12: The feasibility ratio of a low-voltage grid under different dependence scenarios.

In S_{indep}, failure of a grid node did not cause failure of its corresponding ICT node, because its ICT node has a backup power supply. Hence, the ICT node survived to report the failure of the grid node to the MDMS, and the MDMS assigned convenient loads at the nodes in the low-voltage grid to compensate the absence of the failed grid node, thereby avoiding performance deterioration. In $S_{partial\_Dep}$, a failure of a grid node caused failure of its corresponding ICT node, which led to cascaded failures. Even worse, a failure of a grid node in S_{full_Dep} caused failure of the grid node that supplies power to the RN that led to failure of the RN itself. With the failure of the RN, the ICT nodes that it covers were not able to reach the MDMS. Hence, the MDMS undertook load allocations by assuming ex-

pected values for many nodes whose ICT nodes could not be reached, leading to larger performance deterioration compared to $S_{partial\_Dep}$. This clearly reveals that failure of the RN has huge impact on performance of the grid, hence, allocating it a backup power supply can gain large improvement in the reliability of the power grid.

We have also conducted simulations that revealed that the larger the number of ICT nodes with backup power supplies, the better is the performance of the power grid, because then the possibility of cascaded failure is reduced. However, allocating a backup power supply for each ICT node increases the cost of deploying the ICT network. Throughout all our simulations, in response to a failure of an ICT or a power network node, operational boundaries of voltage levels occurred mostly at the grid nodes that are located at a larger electrical distance from the transformer, due to voltage drops in the cables. Thus, making the ICT nodes at the power grid nodes that are further from the transformer independent from the power grid could help avoid cascading failures.

4.3. Optimal interdependency design

Here, we use the findings of our simulation results to propose a metric that quantifies the resilience of the two interdependent networks in terms of the properties of the nodes in both networks. *First*, our findings show that failure of an information relay node of the ICT network leads to a larger performance deterioration than does a failure of an ICT node at a house. Accordingly, an important property of an ICT node is the number of grid nodes that communicate with the MDMS through the ICT node. We refer to this property as the *betweenness* of the ICT node, denoted by B. Thus, the betweenness of an ICT node at a house is 1, while that of an information relay node is equal to the total number of houses it is covering.

Second, making the ICT nodes of the houses located at large electrical distance from the transformer dependent on the grid nodes increases vulnerability to cascading failures compared to doing the same for ICT nodes of the houses that are closer to the transformer. Thus, an important property of a grid node is its *distance from the transformer*, denoted by Z, which can be expressed as the electrical impedance between the grid node and the transformer. We normalize both Z and B: Z is normalized by the largest Z of all the nodes, and B by the total number of grid nodes.

Third, failures cascade further when more ICT nodes depend on grid nodes, thus more ICT nodes need to be independent to improve performance.

Accordingly, we model the significance of the impact of failure of a grid node on the performance of the interdependent networks by a metric *grid-*

node-significance, Y, given in Eq. 29. In the equation, a is a parameter that represents the availability of the grid node, which is the probability that it operates and does not fail [38]. Thus $(1 - a)$ is its probability of failure. E is a binary variable that is equal to 1 if the corresponding ICT node is dependent on the grid node, or 0 otherwise. Failure of a grid node influences the interdependence only if the corresponding ICT node is dependent on it. B is the betweenness of the ICT node corresponding to the grid node. The larger values of Z and B imply that the grid node has larger impact if its corresponding ICT node is dependent, i.e., the ICT node does not have backup power supply. Likewise, the significance of the impact of failure of an ICT node, ICT-node-significance (Y^*), is given in Eq. 30, where a^* is the availability of the ICT node. The grid node is always dependent on the corresponding ICT node, and the significance of an ICT node is larger when it has larger betweenness.

$$Y = (1 - a) \times E \times Z \times B \tag{29}$$

$$Y^* = (1 - a^*) \times Z \tag{30}$$

The overall vulnerability (Q) of the interdependent networks to failure of the ICT and grid nodes can be obtained by summing Y^G and Y^I over all the grid and ICT nodes, as shown in Eq. 31. We define the interdependent resilience, U, of the networks as a function of the vulnerability of the system as shown in Eq. 32.

$$Q = \sum_{j=1}^{N} (Y_j + Y_j^*) \tag{31}$$

$$U = 1 - Q \tag{32}$$

Clearly, U can be increased by making more ICT nodes independent of the grid. However, this incurs more cost because a backup battery is required to make the ICT node independent. A network designer needs to achieve a desirable performance with minimal cost. Next, we propose a design algorithm (Algorithm 1) that guarantees the minimal bound on the resilience R, with minimum number of independent ICT nodes. The algorithm starts by setting all ICT nodes dependent on the grid (line 1). After sorting the nodes in descending order in terms of their Y_j (line 4), the algorithm repeatedly makes the node with the largest Y_j independent from the grid until the required minimum bound (β) on resilience is achieved (line 5 - 10).

Fig. 13 shows the resilience as a function of the number of independent ICT nodes, for different values of a and a^*. In the figure, the resilience rises

Algorithm 1 Algorithm for optimal design of ICT node dependence on power grid.

Initialize $E_j = 1$, $\forall j \in \{1, 2, ..., N\}$
Compute Y_j, Y_j^*, $\forall j \in \{1, 2, ..., N\}$
Compute Q and Q^{indep}
Sort $\{Y_j\}$ in decreasing order, and store it in the list A
repeat
    remove the node at the front of A, and let $m =$ the id of the removed node
    $E_m = 0$
    $Q = Q - Y_m$
    Compute U
until $U \geq bound$

significantly when the first ICT node is made independent, which is the information relay node. Afterwards, the improvement in resilience becomes smaller as more ICT nodes are made independent. Since the ICT nodes located at houses closer to the transformer have lower impact $(Y + Y^*)$, making them independent yields lower level of improvement.

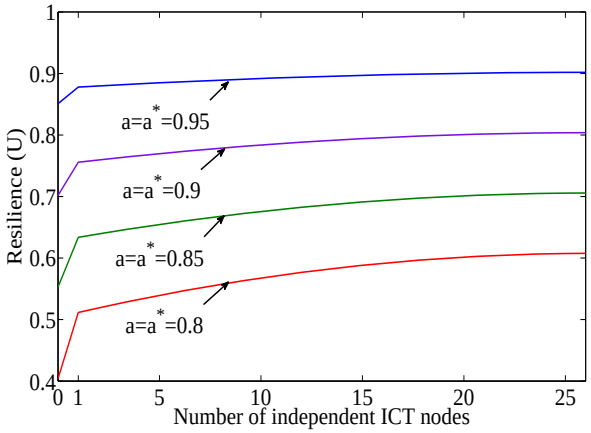

Figure 13: The resilience of the low-voltage grid as a function of the number of independent ICT nodes.

5. Conclusion

With the increasing availability of distributed energy sources and new devices that consume large amounts of power, the load profiles at the end customers of the electric power system will change significantly. However, the structure of the low-voltage grid was originally designed for end customers with conventional small loads. Hence, the topological structure of the low-voltage grid needs to be re-evaluated to accommodate this. Moreover, the bidirectional interdependence between the low-voltage grid and its supporting ICT network raises concerns about the reliability of the low-voltage grid. This paper has addressed the two issues: assessing the structure of the low-voltage grid, and analyzing the impact of the interdependence between the two networks on the reliability of the low-voltage grid.

We have conducted a novel study on how the structural features of a low-voltage grid influence its operational performance. With this study, we have identified the influential structural properties of the low-voltage grid to optimize its operational performance. Moreover, we have proposed metrics that capture the resilience of a low-voltage grid to link failures. Our resilience metrics reflect the unique connectivity features of a low-voltage grid. Based on this, we have proposed a constraint programming formulation for a minimal-cost design of a low-voltage grid topological structure that optimizes the structural metrics that influence its operational performance.

Our study has asserted that the radial structure that is traditionally used to design low-voltage grids cannot accommodate the new load profiles. Thus, the low-voltage grids need to be redesigned. A low-voltage grid designer is advised to optimize the influential structural features identified in this study, as presented in our design formulation of the low-voltage grid.

Our analysis on the impact of the interdependence between the low-voltage grid and ICT network indicates that the more ICT nodes depend on the low-voltage grid for their power supply, the lower the reliability of the low-voltage grid. Moreover, we have found that the betweenness of the ICT node and the distance of the grid node from the transformer influence the extent of the impact a failure of a grid/ICT node would have on the operational performance of the low-voltage grid. Based on this, we have proposed an algorithm that designs an optimal level of dependence of ICT nodes on the low-voltage grid.

The objective of this algorithm is to minimize the number of ICT nodes that depend on the low-voltage grid as much as possible to increase the reliability of the grid. In addition, the algorithm allows to increase the reliability of the grid by making the information relay nodes and the ICT

nodes of the houses located at large electrical distance from the transformer independent of the grid for their power supply.

6. Acknowledgement

We thank Alliander for having provided us with data. Part of this work has been supported by the EU FP7 EINS project under grant agreement No. 288021.

References

[1] Y. Yan, Y. Qian, H. Sharif and D. Tipper, A survey on smart grid communication infrastructures: motivations, requirements and challenges, *IEEE Communications Survey & Tutorials*, vol. 15(1), pp. 5–20, 2012.

[2] G. D'Agostino, S. Bologna, V. Fioriti, E. Casalicchio, L. Brasca, E. Ciapessoni and S. Buschi, Methodologies for inter-dependency assessment, *IEEE fifth International Conference on Critical Infrastructure*, pp. 1–7, 2010.

[3] D. Niyato and P. Wang, Reliability analysis and redundancy design of Smart Grid Wireless Communications System for Demand Side Management, *IEEE Wireless Communications*, vol. 19(3), pp. 38–46, 2012.

[4] R. Albert and A.L. Barabási, Statistical mechanics of complex networks, *Reviews of Modern Physics*, vol. 74(1), pp. 47, 2002.

[5] E. Bompard, E. Pons and D. Wu, Analysis of the structural vulnerability of the interconnected power grid of continental Europe with the Integrated Power System and Unified Power System based on extended topological approach, *European transactions on Electrical Energy Systems*, vol. 23(5), pp. 620 – 637, 2013.

[6] G. A. Pagani and M. Aiello, Towards decentralization: a topological investigation of the medium and low voltage grids, *IEEE transactions on Smart Grids*, vol. 2(3), pp. 538–547, 2011.

[7] R. Albert, I. Albert and G. L. Nakarado, Structural vulnerability of the North American power grid, *Physical Review E*, vol. 69(2), pp. 025103, 2004.

[8] P. Crucitti, V. Latora and M. Marchiori, Topological analysis of the Italian electric power grid, *Physica A: Statistical mechanics and its applications*, vol. 338(1), pp. 92–97, 2004.

[9] Z. Wang, A. Scaglione and R. J. Thomas, Generating statistically correct random topologies for testing smart grid communication and control networks, *IEEE transactions on Smart Grid*, vol. 1(1), pp. 28–39, 2010.

[10] E. Bompard, R. Napoli and F. Xue, Extended topological approach for the assessment of structural vulnerability in transmission networks, *IET Generation, Transmission and Distribution*, vol. 4(6), pp. 716–724, 2010.

[11] E. Cotilla-Sanchez, P.D.H. Hines, C. Barrows and S. Blumsack, Comparing the topological and electrical structure of the North American electric power infrastructure, *IEEE Systems Journal*, vol. 6(4), pp. 616–626, 2012.

[12] I. Dobson, B. Carreras, V. Lynch and D. Newman, Complex systems analysis of series of blackouts: Cascading failure, critical points, and self-organization, *Chaos: An Interdisciplinary Journal of Nonlinear Science*, vol. 17(2), pp. 026103, 2007.

[13] D. Chassin and C. Posse, Evaluating north American electric grid reliability using the BarabasiAlbert network model, *Physica A: Statistical Mechanics and its Applications*, vol. 355(2), pp. 667-677, 2005.

[14] R. Sole, M. Rosas-Casals, B. Corominas-Murtra and S. Valverde, Robustness of the European power grids under intentional attack, *Physical Review E*, vol. 77(2), pp. 026102, 2008.

[15] J. Wang and L. Rong, Cascade-based attack vulnerability on the U.S. power grid, *Safety Science* vol. 47(10), pp. 1332–1336, 2009.

[16] S. Arianos, E. Bompard, A. Carbone and F. Xue, Power grids vulnerability: A complex network approach, *Chaos: An Interdisciplinary Journal Nonlinear Science*, vol. 19(1), pp. 013119, 2009.

[17] D. Ming and H. Ping-Ping, Small-world topological model based vulnerability assessment algorithm for large-scale power grid, *Automation of Electric Power Systems*, vol. 8, pp. 7–10, 2006.

[18] V. Rosato, S. Bologna and F. Tiriticco, Topological properties of high-voltage electrical transmission networks, *Electric Power Systems Research*, vol. 77(2), pp. 99–105, 2007.

[19] A. Holmgren, Using graph models to analyze the vulnerability of electric power networks, *Risk Analysis*, vol. 26(4), pp. 955-969, 2006.

[20] Z. Wang, A. Scaglione and R. Thomas, Electrical centrality measures for electric power grid vulnerability analysis, *Fourty-ninth IEEE Conference on Decisicion and Control*, pp. 5792-5797, 2010.

[21] P. Hines and S. Blumsack, A centrality measure for electrical networks, in *Proceedings of the fourty-first Hawaii International Conference on System Sciences, IEEE*, pp. 185–185, 2008.

[22] P. Hines, S. Blumsack, E. Cotilla-Sanchez and C. Barrows, The topological and electrical structure of power grids, in *Proceedings of the fourty third Hawaii International Conference on System Sciences, IEEE*, pp. 1–10, 2010.

[23] E. Bompard, R. Napoli and F. Xue, Analysis of structural vulnerabilities in power transmission grids, *International Journal of Critical Infrastructure Protection*, vol. 2(1), pp. 512, 2009.

[24] L. Fu, W. Zhang, S. Xiao, Y. Li and S. Guo, Vulnerability assessment for power grid based on small-world topological model, in *Proceedings of IEEE Asia-Pacific Power and Energy Engineering Conference*, pp. 1–4, 2010.

[25] M. Rosas-Casals, S. Valverde and R. Sole, Topological vulnerability of the European power grid under errors and attacks, *International Journal of Bifurcation and Chaos*, vol. 17(7), pp. 24652475, 2007.

[26] Z. Fan, P. Kulkarni, S. Gormus, C. Efthymiou, G. Kalogridis, M. Sooriyabandara, Z. Zhu, S. Lambotharan and W. H. Chin, Smart grid communications: overview of research challenges, solutions, and standardization activities, *IEEE Communications Surveys and Tutorials*, vol. 15(1), pp. 21–38, 2011.

[27] S.V. Buldyrev, R. Parshani, G. Paul, H.E. Stanley and S. Havlin, Catastrophic cascade of failures in interdependent networks, *Nature*, vol. 464(7291), pp. 1025–1028, 2010.

[28] B. Bollobás, *Random Graphs*, Springer New York, 1998.

[29] A. L. Barabási, Scale-free networks: a decade and beyond, *Science*, vol.325(5939), pp. 412, 2009.

[30] D. J. Watts and S. H. Strogatz, Collective dynamics of 'small-world' networks, *Nature*, vol. 393(6684), pp. 440–442, 1998.

[31] L.F. Costa, F.A. Rodrigues, G. Travieso and P.R.V. Boas, Characterization of complex networks: a survey of measurements, *Advances in Physics*, vol. 56(1), pp. 167–242, 2007.

[32] Gaia low-voltage Network Design (`http://www.phasetophase.nl/en_products/vision_lv_network_design.html`)

[33] Mobility Research of The Netherlands 2009 (mobilitietsonderzoek nederland 2009) (`http://rijkswaterstaat.nl/`), 2009.

[34] F.A. Kuipers, An Overview of Algorithms for Network Survivability, ISRN Communications and Networking, vol. 2012, Article ID 932456, 19 pages, 2012.

[35] P. Van Mieghem, C. Doerr, H. Wang, J. Martin Hernandez, D. Hutchison, M. Karaliopoulos and R.E. Kooij, A framework for computing topological network robustness, Delft University of Technology, Report20101218, 2010.

[36] E. Negeri and N. Baken, Distributed storage management using dynamic pricing in a self-organizing energy community, in *Proceedings of sixth International Workshop on Self Organized Systems*, pp. 1–12, 2012.

[37] A. Athreya and P. Tague, Survivable smart grid communication: smartmeters meshes to the rescue, *IEEE International Conference on Computing, Networking and Communications*, pp. 104–110, 2012.

[38] W. Zou, M. Janic, R. Kooij and F.A. Kuipers, On the availability of networks, in *Proceedings of BroadBand Europe*, 2007.